An Integrated Frequency Reconfigurable Antenna for Cognitive Radio Application

Sonia SHARMA, Chandra Charu TRIPATHI

Dept. of Electronics and Communication Engineering, UIET, Kurukshetra University, Kurukshetra, India

sonia990@gmail.com, tripathiuiet@gmail.com

Submitted November 20, 2016 / Accepted May 22, 2017

Abstract. *A novel integrated antenna that consists of spectrum sensing and frequency reconfigurable antenna, printed on a single substrate is presented here. The integration of both antennas is based on the fact that reasonably large metallization area of UWB antenna can be used as a space for printing another narrowband antenna. Prominently, the second antenna should be placed on a region of large UWB antenna where there is less distribution of E field. The proposed antenna senses the spectrum over a wide frequency range from 2 GHz to 12 GHz via a U shape monopole having partial ground structure. After sensing the spectrum condition, the slot antenna with reconfigurable feeding structure can switch its operating bands among six narrowbands: 5.65 GHz, 3.6 GHz, 5 GHz, 2.94 GHz, 4.5 GHz, 2.15 GHz and two dual bands at 2 GHz, 5.48 GHz and 1.7 GHz, 5 GHz. In addition to this, the proposed antenna can also reconfigure its frequency in wide-bandwidth using two ground stubs. Since wide band response for spectrum sensing and each of eight frequency state works independently, therefore, there is no interference among various signals.*

Keywords

Cognitive radio, frequency reconfiguration, slot antenna, spectrum sensing, wideband antenna

1. Introduction

The next generation smart systems should have capability to automatically detect the spectrum condition and accordingly change the radio operating parameters to modify system performance such as maximize throughput, mitigate interference, facilitate interoperability etc. In addition, the physical size of these devices must follow the downsizing trend of the system unit. A smart Cognitive Radio (CR) compatible antenna with smaller physical size meets the essential requirement for these systems. Such antenna has a spectrum-sensing antenna for detecting the spectrum condition and reconfigurable antenna for communicating purpose [1], [2]. Many antenna designs have been already reported in the literatures, which are compatible with CR [3–6]. Further to decrease the system size, these two antennas must be optimally design on a single substrate. Only a handful of techniques based on integration concept of these antennas, on a single substrate are reported in literature [7–15]. In these techniques, small narrowband (NB) antenna are integrated in UWB antenna by using various topology viz. using large metallization area of UWB antenna as ground plane for a smaller antenna [7], [8], by utilizing the empty space in between the radiating element, and in between two tapered slots [9], by adding reconfigurable part in the feeding area of Vivaldi antenna [10], by adding reconfigurable band pass filter in feed line [11], by adding JK inverter in the switchable feed line structure [12], by placing the NB antenna at a point where electric field does not disturb the UWB antenna [13], by adding UWB antenna above the reconfigurable antenna [14], by reusing the printed area in different operating modes [14], etc. In all the above designs the numbers of frequency reconfiguration states are limited because of size constraint so there is underutilization of available area. Further up gradation of these antennas to increase the reconfiguration states is quite challenging because of limited space constraints on board. This may compromise the goal of combining the wideband and reconfigurable antenna together for CR systems.

Therefore, in the present work, UWB antenna and reconfigurable antenna are integrated in such a way that they do not disturb the characteristics of each other. The challenging goal in this work is to use the available space optimally for multiple purposes. For space management, the

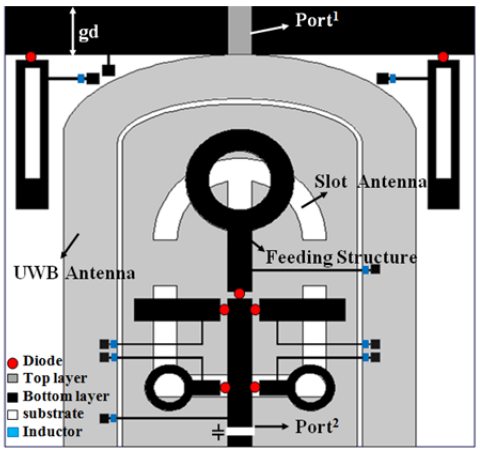

Fig. 1. Layout of the proposed integrated antenna.

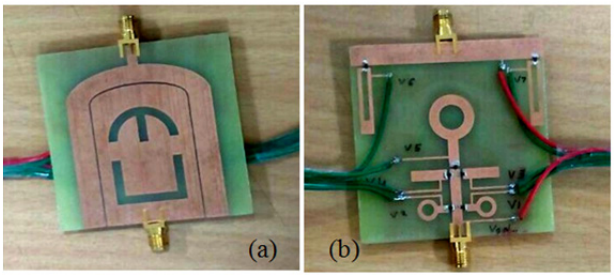

Fig. 2. Fabricated prototype: (a) Top view. (b) Bottom view.

large metal area of UWB antenna can be used for printing slot antenna and the partially etched ground area can be used for printing reconfigurable feeding structure for the slot antenna. Proper isolation of high field and low field area ensure the least interaction between two antenna and efficient utilization of space for multipurpose.

2. Design Strategy/Design Evolution

For CR systems, an antenna consists of two parts: a UWB antenna as a spectrum sensor and a reconfigurable NB antenna for communicating purpose. So, a U shape monopole, which is excited by port[1], is chosen as a spectrum sensor, over a wide spectrum range from 2 to 12 GHz. A reconfigurable slot antenna, which is excited by port[2], is used as communicating antenna in an operating range between 1 GHz to 6 GHz. The target is to integrate these two individual antennas on a single substrate to use the available space optimally such that space of one antenna can be used for printing two antennas. Importantly, the NB antenna should be positioned in a region of the UWB antenna where there is less concentration of electric field intensity. The high and low field areas on the UWB antenna are isolated by etching a thin slit in order to have space for the NB antenna. This ensures less interaction between the two antennas. The corresponding antenna topology is shown in Fig. 1 and the fabricated prototype is shown in Fig. 2. It consists of two layers. The top layer is the large U shape antenna and the bottom layer consists of partial ground plane and reconfigurable feeding structure. The design steps adopted for complete integration topology are explained below.

2.1 Integration Methodology

Here, the methodology adopted to integrate a NB antenna into the large UWB antenna is explained thoroughly. Firstly a U shape monopole antenna namely configuration I is designed on 6×6 cm^2 substrate as shown in Fig. 3(a). The proper selection of monopole shape and partial ground plane size optimizes the impedance bandwidth of UWB antenna. Figure 5 shows the effect of partial ground size on the return loss characteristics in UWB range. The result clearly show that the UWB behavior of antenna improved as we increased the ground plane size from 5 mm to 7 mm. Further increasing the ground size, the UWB response starts degrading, so the optimum size of partial ground plane is chosen as 7 mm for UWB response from 2 to 12 GHz. Figure 4(a) shows the E field distribution in UWB antenna for configuration I. It is observed that the electric field intensity is very high on the outer periphery and very low intensity is found on the central area of the antenna. If one can separate the high E field area from low E field area

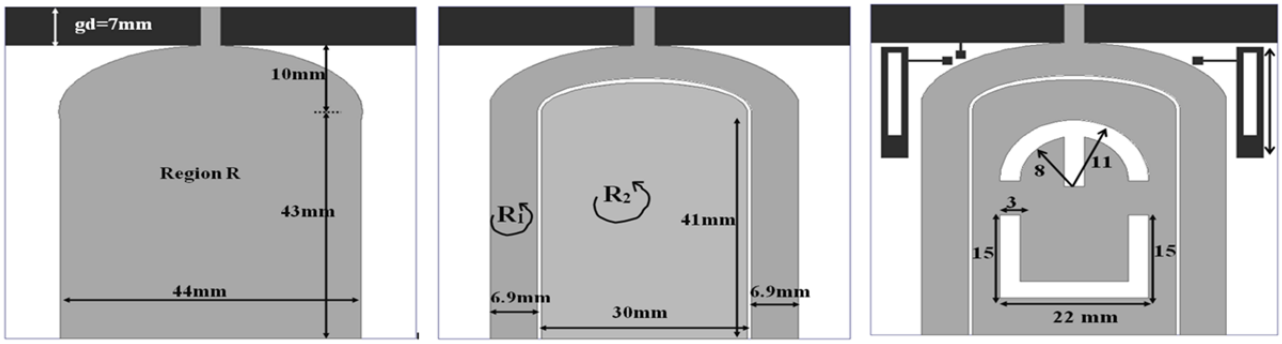

(a) (b) (c)

Fig. 3. Layout of UWB antenna for (a) Configuration I, (b) Configuration II, (c) Configuration III.

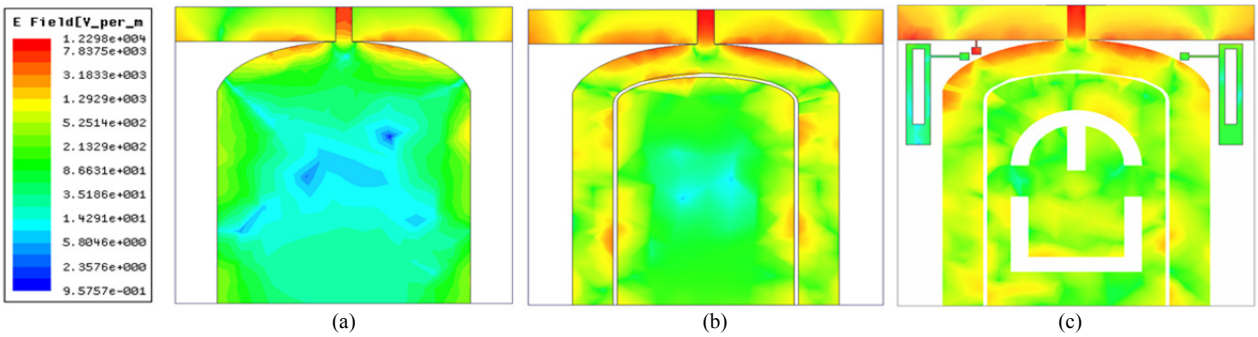

(a) (b) (c)

Fig. 4. E field distribution in (a) Configuration I (b) Configuration II, (c) Configuration III.

in UWB monopole without much affecting the S_{11} response, than this space can be reused to integrate another NB antenna. Therefore, in configuration-II a very thin slit is etched in the UWB antenna, which separates the region R into two parts R_1 as high E field area, R_2 very low E field area as shown in Fig. 3(b). The E field distribution for configuration-II is supporting the statement that region R_2 can act as nearly passive area for integrating another antenna. Figure 6 shows that S_{11} parameter from configuration I to II does not disturb so much and is acceptable of UWB operation from 2 GHz to 12 GHz.

Now, in configuration III, two slot antennas (U shape, inverted E shape) are successfully integrated in region R_2 without disturbing the UWB behavior. This configuration is used for spectrum sensing mode and its functioning is explained in detail later. All simulations are done using HFSS ver. 16. Figure 4 shows the E field distribution for all the three configurations and Figure 6 shows the comparisons of S_{11} parameter.

2.2 Mutual Coupling between Ports

In the proposed design, the UWB and the reconfigurable antenna are integrated together but work independently because both antennas are excited by different ports, one at a time. Both operating modes work separately without interfering each other's characteristics. Further, design optimization of integrated antenna is done so that passive

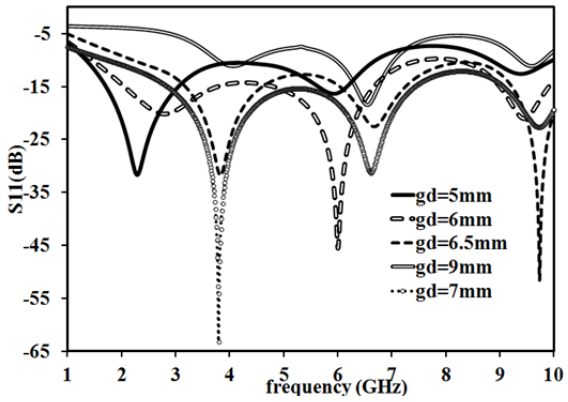

Fig. 5. Effect of ground plane size on UWB characteristics.

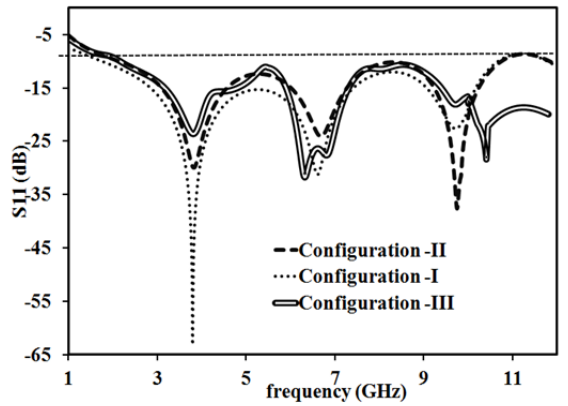

Fig. 6. Comparison of S_{11} vs. freq. for Configuration I, II, III.

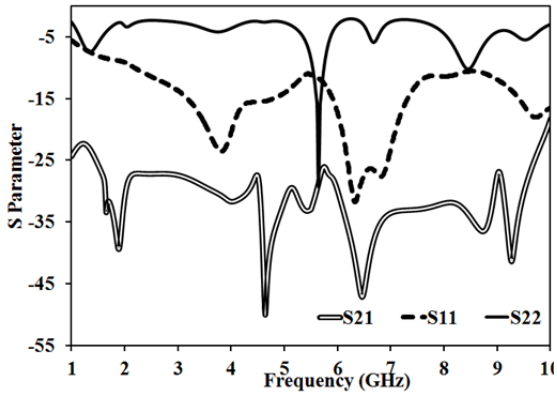

Fig. 7. *S* parameter (dB) vs. frequency for port isolation.

antenna does not interrupt the operating state of active antenna. To prove that both antennas do not interfere with each other's characteristics, coupling coefficient for both the ports are studied.

Figure 7 shows the simulated *S* parameter. The response clearly shows that S_{21} is better than 25 dB from 2 to 12 GHz, which proves that there is no transmission of RF power from port[1] to port[2]. So there is no need to design extra port isolation circuit because there is good isolation in both operating modes and this ensures no interaction of both the antennas.

3. Antenna Architecture and Working Operation

Now antenna architecture, geometry description and working for each mode is explained in detail below.

3.1 UWB Antenna Design

Figure 8 shows the active portion of integrated antenna when operated in spectrum sensing mode (configuration III). In this mode, antenna is fed by port[1] to excite the U shape monopole. The top layer structure consists of U shape monopole and bottom layer consists of partial ground and two symmetrical stubs (S_6, S_7). The two ground stubs namely S_6, S_7 are used to reconfigure the frequency in wideband (WB) mode. Diode D_6 and D_7 are used to control the state of stubs S_6 and S_7 independently. Three modes

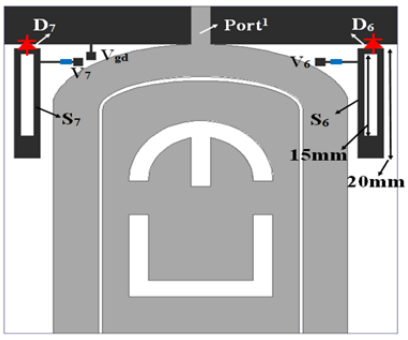

Fig. 8. Active area of integrated antenna in UWB mode.

have been studied using different combination of D_6 and D_7. When both diodes are in OFF state then UWB antenna operates in Spectrum Sensing mode from 2 to 12 GHz. When either one of the diode D_6 or D_7 is ON by applying +5 V on V_6 or V_7 pad then UWB antenna operates in WB mode-I. If both diodes D_6 and D_7 are forward biased by applying +5 V onV_6 and V_7 DC pad then UWB antenna operates in WB mode-II.

3.2 Frequency Reconfigurable Antenna Design

Figure 9 shows the active portion of the integrated antenna when it operates in frequency reconfigurable mode. The two slot antennas are imprinted such that they use switchable feed line structure for their active operation. Figure 9(b) shows feeding structure which is composed of two feed lines (F_1, F_2), four stubs (S_1, S_2, S_3, S_4), 5 PIN Diodes (D_1, D_2, D_3, D_4, D_5) and 6 DC pads (V_1, V_2, V_3, V_4, V_5, V_{gd}). The heart of the proposed design is electronically switchable feeding structure, which is specially designed for frequency reconfiguration using micro strip open stubs. These stubs are placed at proper position, such that these stubs match the antenna's input impedance at different desired frequencies. Five PIN diodes are used to control the activation of different stubs independently. The diode positioning along with DC biasing network are given in Fig. 9(b). The orientations of all PIN diodes are such that they share single ground pad. Applying 5 voltages on their respective DC pad and ground signal on V_{gd} pad activate the respective PIN diodes.

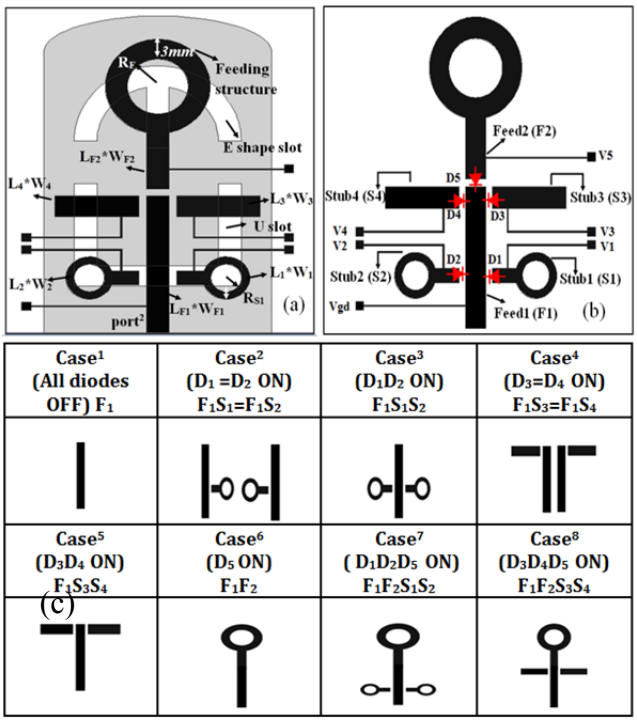

Fig. 9. Active area of integrated antenna in frequency reconfigurable mode, (b) layout of reconfigurable feeding network, (c) different cases using different diode combinations.

F_1	$Stub^1$=$Stub^2$	$Stub^3$=$Stub^4$	F_2	R_{S1}, R_F
$L_{F1} \times W_{F1}$ 20 × 3	$L_1 \times W_1$ = $L_2 \times W_2$ = 4.56 × 3	$L_3 \times W_3$ = $L_4 \times W_4$ = 12 × 3	$L_{F2} \times W_{F2}$ 9.23 × 3	2, 3

Tab. 1. Geometrical parameter of the feeding structure (mm).

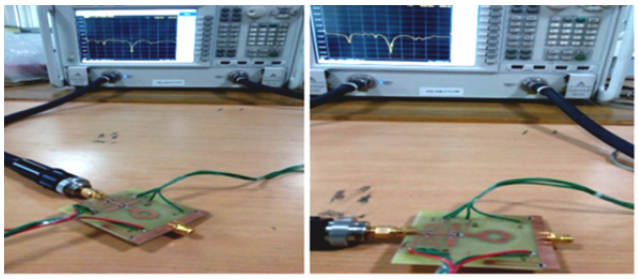

Fig. 10. Experimental setup for the integrated antenna.

A number of cases for different combination of these diodes can be envisaged. Figure 9(c) shows the diode state and pictorial view of active portion of feeding structure under different cases. When no diode is forward biased than feed line portion F_1 excites the lower U slot antenna ($case^1$). Now by activating different stubs combination with feed line F_1, lower U slot antenna can reconfigure its resonant frequency over 4 different bands ($case^2$ - $case^5$). When diode D_5 is forward biased than feed line portion F_1F_2 also excites the upper E shaped slot antenna ($case^6$). For this combination two cases are also discussed, i.e. when stub S_1 and S_2 are attached with feed line F_1F_2 ($case^7$) and stub S_3 and S_4 are attached with the feed line portion F_1F_2 ($case^8$). The geometrical parameters for the reconfigurable feeding structure are given in Tab. 1.

4. Results and Discussion

To validate the proposed design, the prototype has been fabricated and results are verified experimentally here. Figure 10 shows the experimental setup for integrated antenna. In the prototype, Infineon BAR-6402 diodes are used here. In Ansoft HFSS 16, PIN diodes are model using lumped RLC boundary to add the effect of actual diodes.

4.1 Spectrum Sensing Mode/ WB Frequency Reconfigurable Mode

Antenna works in normal mode or spectrum sensing mode, when both stubs (S_6, S_7) are not attached with the partial ground structure (D_6 D_7 -00). Figure 11 shows the simulated and measured S_{11} vs. frequency for normal mode. It is clear that simulated and measured S_{11} is better than –10 dB in UWB bandwidth from 2 GHz to 10 GHz. Figure 11 also shows the very low electric field distribution is observed in the central part of the antenna and maximum on the outer edges of the U shape monopole.

The gain of the antenna is 2.6 dB at 5 GHz as shown in Fig. 12(a). The E and H plane pattern is nearly omnidirectional except a discontinuity at $\theta = 180°$. Figure 12(b) shows the simulated and measured E plane pattern at 5 GHz.

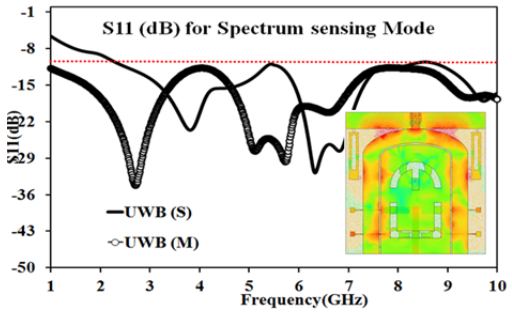

Fig. 11. S_{11} vs. frequency in normal mode.

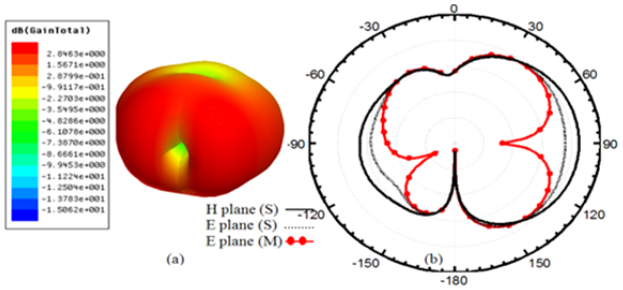

Fig. 12. (a) Gain polar plot. (b) Observed radiation pattern at 5 GHz.

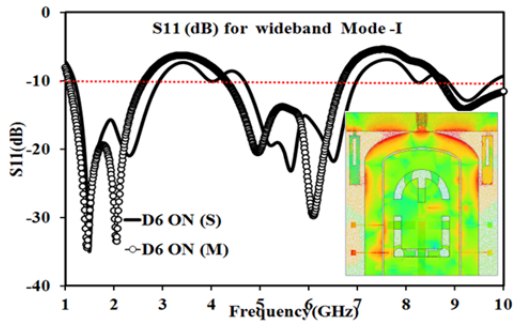

Fig. 13. S_{11} vs. frequency in wideband mode- I.

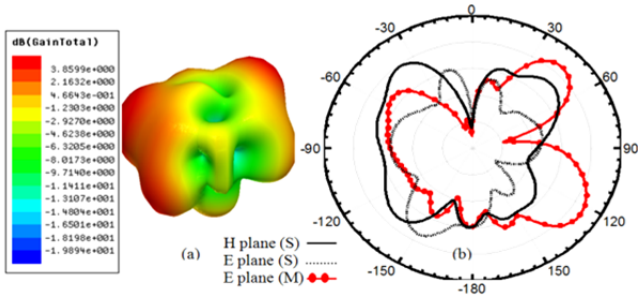

Fig. 14. (a) Gain polar plot, (b) Observed radiation pattern at 5 GHz.

When diode D_6 is forward biased, then stub S_6, reconfigures the operating bandwidth and the antenna works for WB-I. Now the antenna has two WBs from 1 to 3 GHz and from 5 to 7 GHz as shown in Fig. 13. Simulated and measured S_{11} is better than –10 dB for 1–3 GHz and 5–7 GHz. Figure 13 shows that E field redistributes under UWB antenna and stub S_6. The observed value of gain is 2.4 dB at 5 GHz as shown in Fig. 14(a). Simulated and measured radiation pattern at 5 GHz has distorted shape as shown in Fig. 14(b). If both diodes D_6 and D_7 are forward

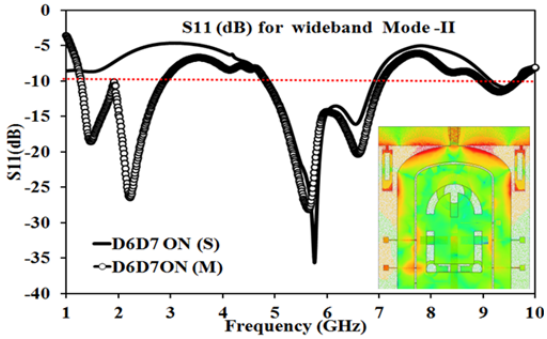

Fig. 15. S_{11} vs. frequency in wideband mode-II.

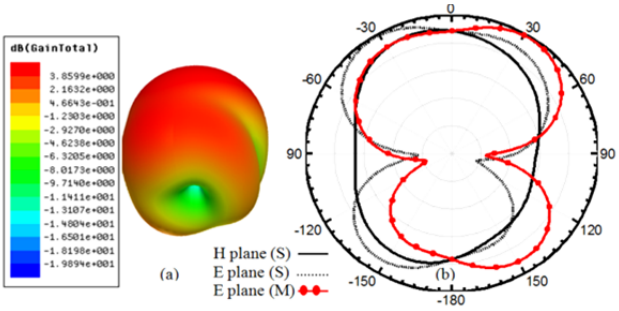

Fig. 16. (a) Gain polar plot, (b) Observed radiation pattern at 5 GHz.

biased then stub S_6 and S_7 are attached with the partial ground to tune the operating bandwidth.

In this case, the antenna operates in WB-II. Simulated and measured S_{11} is better than –10 dB from 5 to 7 GHz. Figure 15 also shows that E field redistributes and the maximum field is found under UWB antenna and stubs S_6 and S_7. In this case, the maximum value of gain is 3.6 dB as shown in 3D polar plot of gain in Fig. 16(a). The shape of H plane is nearly omni-directional and E plane is nearly dumbbell-shaped as shown in Fig. 16(b).

4.2 NB Frequency Reconfigurable Mode

In this mode, different combinations of stubs are activated at different times to achieve frequency reconfiguration. All the cases are discussed by comparing simulated S_{22} with the measured value and analyzing electric field distribution. The 3D polar plot for gain and simulated and measured radiation pattern for each mode is also given for each frequency state. In case[1], when all the diodes are in OFF condition then feedline section F_1 excites the U slot structure. Figure 17(a) shows the simulated and measured S_{22} vs. frequency for this case. The simulated value of return loss (RL) is 30 dB at resonating frequency 5.65 GHz whereas the measured value of RL = 28 dB at 5.68 GHz. Electric field distribution for case[1] is also given in Fig. 17(a) which clearly shows that maximum E field is distributed under F_1 portion. The observed value of gain is 3.43 dB and comparison of simulated and measured radiation pattern is shown in Fig. 17(b-c) respectively. In case[2], either of diode D_1 or D_2 is forward biased by applying +5 V on V_1 or V_2 pad then antenna resonates at 3.6 GHz as shown in Fig. 18. In this case, the U slot antenna is fed by

feedline section F_1 in conjunction with stub[1] or stub[2]. It should be noted here that resonating frequency for feedline structure F_1S_1 or F_1S_2 is found the same because geometry of stub[1] and stub[2] are identical so they are symmetrically placed across feedline section F_1. In this case, the simulated frequency is 3.6 GHz with *RL* = 28.3 dB whereas the measured frequency is 3.69 GHz with *RL* = 40 dB as shown in Fig. 18. The maximum E field intensity is found under F_1S_1 structure. The observed value of gain is 2.8 dB and simulated and measured radiation patterns are shown in Fig. 18(c) respectively.

In case[3], when diode D_1 and D_2 is forward biased by applying +5 V on DC pad V_1 and V_2 then active feed portion is F_1 along with stub[1] and stub[2]. In this case, the simulated frequency is 5 GHz with *RL* = 30 dB whereas the measured frequency is 5.15 GHz with *RL* = 30 dB as shown in Fig. 19. In this case, electric field is maximum under the $F_1S_1S_2$ structure and at the corner of the U slot antenna. The observed value of gain is 2.7 dB. The simulated and measured radiation patterns are shown in Fig. 19(c).

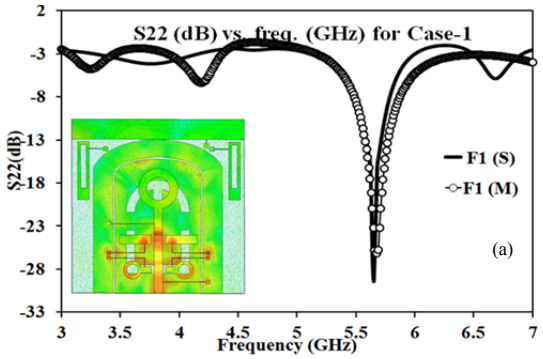

Fig. 17(a) S_{22} vs. frequency for case[1].

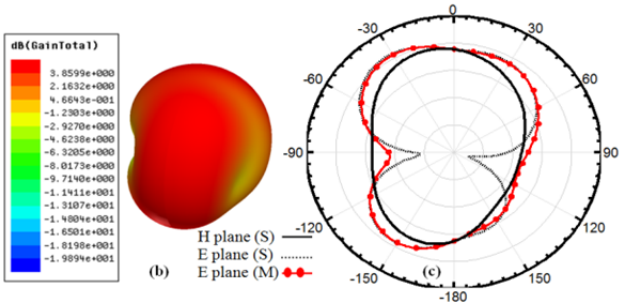

Fig. 17(b) Gain polar plot. **(c)** Observed radiation pattern for case[1].

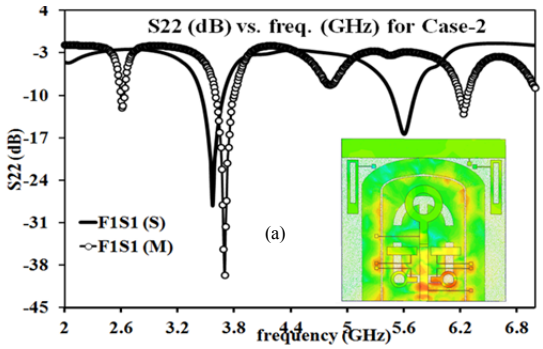

Fig.18(a) S_{22} vs. frequency for case[2].

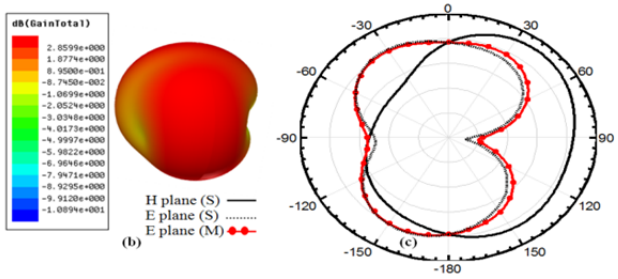

Fig. 18(b) Gain polar plot. **(c)** Observed radiation pattern for case[2].

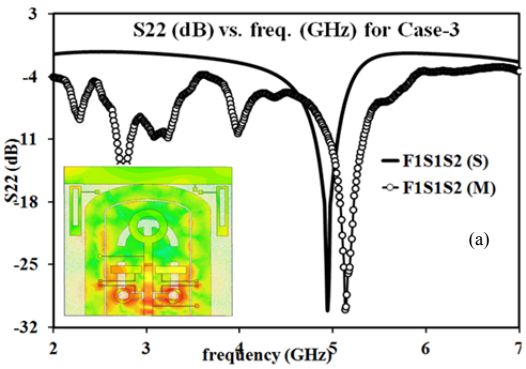

Fig. 19(a) S_{22} vs. frequency for case[3].

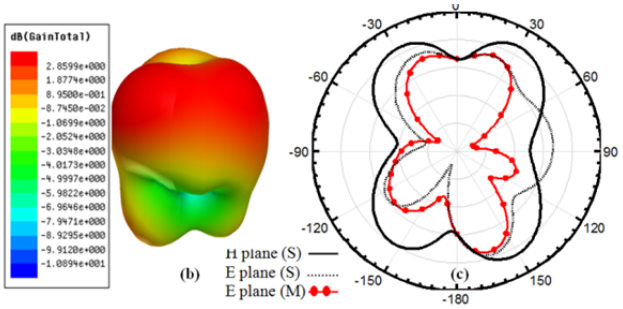

Fig. 19(b) Gain polar plot. **(c)** Observed radiation pattern for case[3].

In case[4], when either of diode D_3 or D_4 is forward biased then either stub[3] or stub[4] is selected to tune the resonating frequency for dual band. Again in this case, due to the geometrical symmetry of F_1S_3 or F_1S_4 structure because of the same geometrical parameters of stub[3] and stub[4], their resonating frequency is found the same for both cases. So only the results for F_1S_3 are given here. In this case, simulated dual band is found at 2 GHz and 5.48 GHz with *RL* = 36 dB, and 35 dB respectively and the measured dual band is obtained at 1.89 and 5.38 GHz with *RL* =27 and 38 dB, respectively, as shown in Fig. 20(a). The observed value of gain is 2.2 dB and the simulated and measured radiation patterns are shown in Fig. 20(c), respectively. The discrepancies between the simulation and measurement radiation patterns can be attributed to the presence of the diodes, in close proximity to the antenna during the pattern measurements.

In case[5], when diode D_3 and D_4 are forward biased by applying +5 V on DC pad V_3 and V_4, then the U slot is excited by T shape feedline structure ($F_1S_3S_4$). In this case, the simulated resonating frequency is 2.94 GHz with *RL* =

34 dB whereas the measured frequency is 3 GHz with *RL* = 35 dB as shown in Fig. 21(a). The electric field is found high under $F_1S_3S_4$ structure as shown in Fig. 21(a). The observed value of gain is 3.7 dB and radiation patterns are shown in Fig. 21(c).

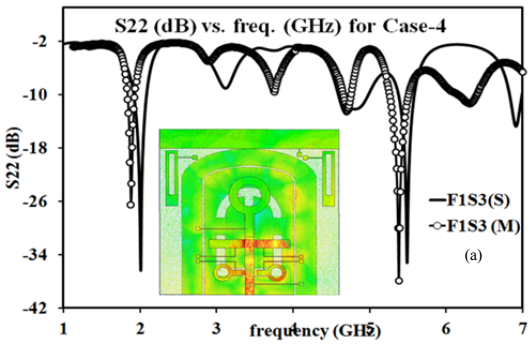

Fig. 20(a) S_{22} vs. frequency for case[4].

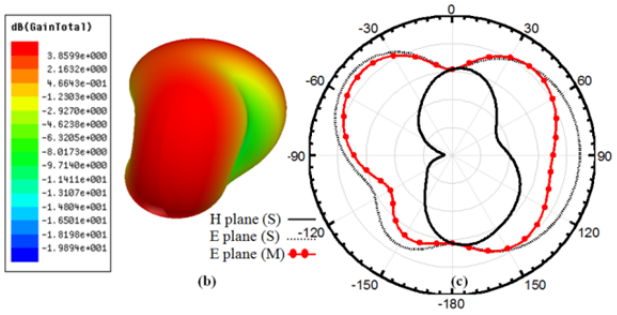

Fig. 20(b) Gain polar plot. **(c)** Observed radiation patterns for case [4].

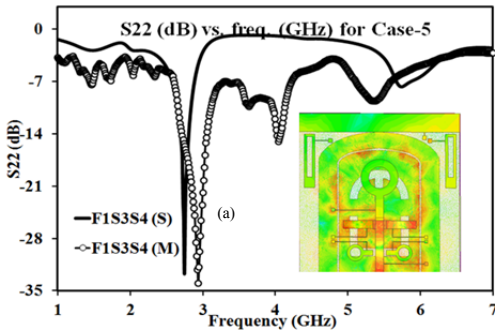

Fig. 21(a) S_{22} vs. frequency for case[5].

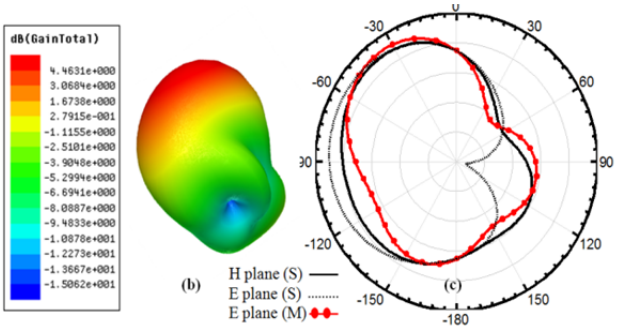

Fig. 21(b) Gain polar plot. **(c)** Observed radiation pattern for case[5].

In case[6], upper inverted E shaped slot is excited by feed line F_1F_2 by forward biasing the diode D_5. The antenna this time resonates at 4.48 GHz with *RL* = 36 dB whereas the measured resonating frequency is 4.5 GHz with *RL* = 40 dB as shown in Fig. 22(a). The observed value of gain is 1.8 dB and radiation patterns are shown in Fig. 22(b-c).

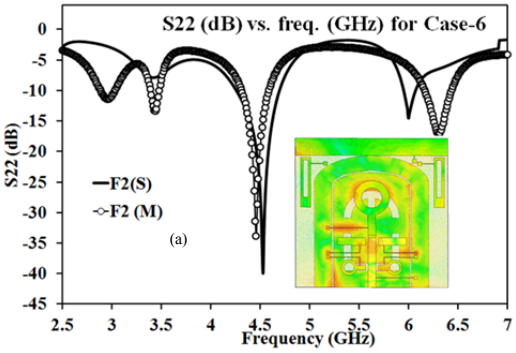

Fig. 22(a) S_{22} vs. frequency for case[6].

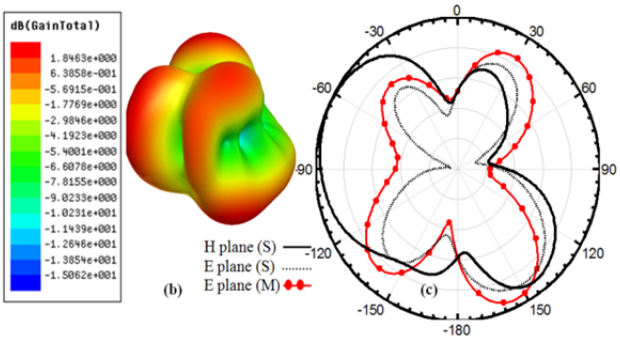

Fig. 22(b) Gain polar plot. **(c)** Observed radiation patterns for case[6].

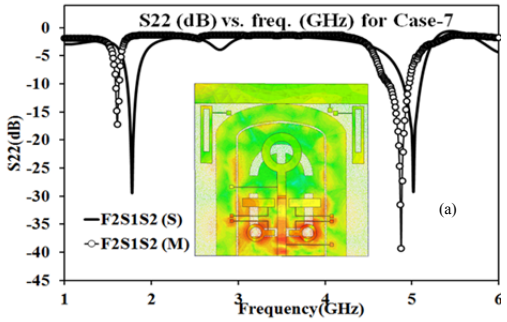

Fig. 23(a) S_{22} vs. frequency for case[7].

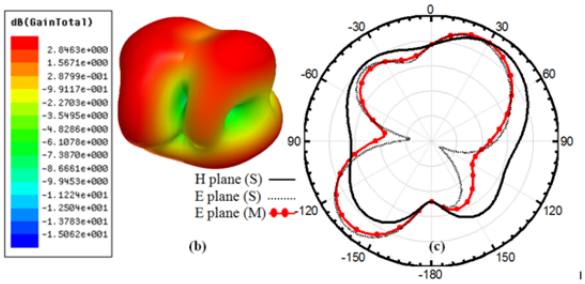

Fig. 23(b) Gain polar plot. (c) Observed radiation patterns for case[7].

In case[7], when diode D_1, D_2, D_5 is forward biased then the slot antenna is excited by feed line section F_1F_2 in conjunction with stub[1] and stub[2]. The electric field distribution for this case is given in Fig. 23(a), which clearly indicates that maximum electric intensity is found under $F_1F_2S_1S_2$ structure. The simulated dual band is found at 1.7 GHz and 5 GHz with the measured *RL* = 30 dB and 31 dB respectively whereas the measured dual band is at 1.66 GHz and 4.88 GHz with *RL* = 18 dB and 31 dB respectively as shown in Fig. 23(a). The observed value of gain is 2.7 dB and the simulated and measured radiation patterns are shown in Fig. 23(c).

In case[8], feed line section $F_1F_2S_3S_4$ excites the slot antenna by forward biasing the diodes D_3, D_4, D_5. In this case, the antenna resonates at 2.15 GHz with *RL* = 38 dB whereas the measured *RL* = 27 dB is at 2 GHz as shown in Fig. 24(a). E field distribution also shows that maximum field is distributing under $F_1F_2S_3S_4$ structure. The observed value of gain is 1.7 dB and the simulated and measured radiation patterns are shown in Fig. 24(c). Simulated and measured parameters are also tabulated in Tab. 2.

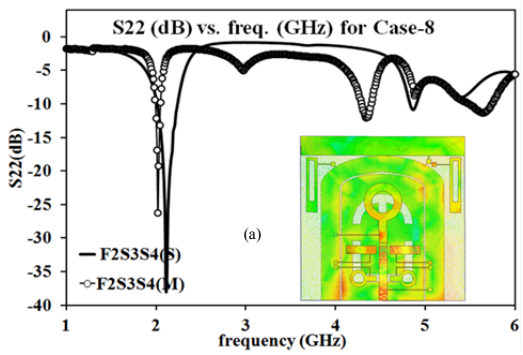

Fig. 24(a) S_{22} vs. frequency for case[8].

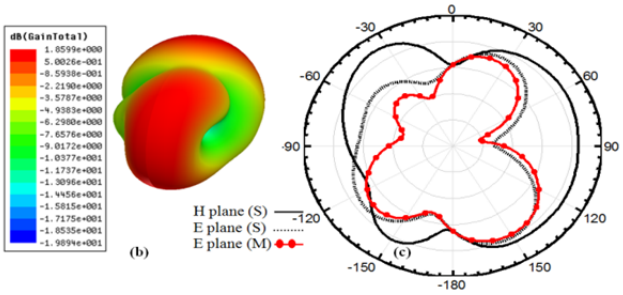

Fig. 24(b) Gain polar plot. **(c)** Observed radiation patterns for case[8].

	Freq. (GHz)	*BW* (MHz)	*RL* (dB)	Eff. η%
Case [1]	5.65	340	30	81
Case [2]	3.6	220	28.3	72
Case [3]	5	260	30	74
Case [4]	2 5.48	160 210	36 35	69 69.8
Case [5]	2.94	190	34	79
Case [6]	4.5	390	40	70
Case [7]	1.7 5	110 210	30 31	71 69
Case [8]	2.15	220	38	67

Tab. 2. Simulated parameters.

5. Conclusion

In this work, we integrate the NB antenna into a large UWB antenna without affecting each performance. The UWB antenna, slot antenna was printed onto the top side of the substrate and the reconfigurable feeding structure for the U slot antenna was printed onto the bottom side of the substrate. This has the advantage of reducing space requirements and making the two antennas lying in the same plane required for cognitive radio communication. The arrangement has potential for various CR applications.

References

[1] HUSSAIN, R., SHARAWI, M. S. A cognitive radio reconfigurable MIMO and sensing antenna system. *IEEE Antennas and Wireless Propagation Letters,* 2015, vol. 14, p. 257–260. DOI: 10.1109/LAWP.2014.2361450

[2] TAWK, Y, CONSTANTINE, J., CHRISTODOULOU, C. G. Cognitive-radio and antenna functionalities: A tutorial. *IEEE Antennas and Propagation Magazine*, 2014, vol. 56, no. 1, p. 231 to 243. DOI: 10.1109/MAP.2014.6821791

[3] SHARMA, S., TRIPATHI, C. C. Frequency reconfigurable U-slot antenna for SDR application. *Progress in Electromagnetics Research Letters,* 2015, vol. 55, p. 129–136. DOI: 10.2528/PIERL15071304

[4] ABOUFOUL, T., ALOMAINY, A., PARINI, C. Reconfiguring UWB monopole antenna for cognitive radio applications using GaAs FET switches. *IEEE Antennas and Wireless Propagation Letters*, 2012, vol. 11, p. 392–395. DOI: 10.1109/LAWP.2012.2193551

[5] TAWK, Y., BKASSINY, M., EL HOWAYEK, G., et al. Reconfigurable front-end antennas for cognitive radio applications. *IET Microwaves, Antennas and Propagation,* 2011, vol. 5, no. 8, p. 985–992. DOI: 10.1049/iet-map.2010.0358

[6] WU, G. T., LI, R. L., EOM, S. Y., et al. Switchable quad-band antennas for cognitive radio base station applications. *IEEE Transactions on Antennas and Propagation*, 2010, vol. 58, no. 5, p. 1468–1476. DOI: 10.1109/TAP.2010.2044472

[7] EBRAHIMI, E., KELLY, J. R., HALL, P. S. Integrated wide-narrowband antenna for multi-standard radio. *IEEE Transactions on Antennas and Propagation*, 2011, vol. 59, no. 7, p. 2628–2635. DOI: 10.1109/TAP.2011.2152353

[8] MANTEGHI, M. A switch-band antenna for SDR applications. *IEEE Antennas and Wireless Propagation Letters*, 2009, vol. 8, p. 3–5. DOI: 10.1109/LAWP.2008.2005256

[9] AUGUSTIN, G., DENIDNI, T. A. An integrated ultra wideband /narrow band antenna in uniplanar configuration for cognitive radio systems. *IEEE Transactions on Antennas and Propagation*, 2012, vol. 60, no. 11, p. 5479–5484. DOI: 10.1109/TAP.2012.2207688

[10] HAMID, M. R., GARDNER, P., HALL, P. S., et al. Vivaldi antenna with integrated switchable band pass resonator. *IEEE Transactions on Antennas and Propagation*, 2011, vol. 59, no. 11, p. 4008–4015. DOI: 10.1109/TAP.2011.2164197

[11] QIN, P. F., WEI, F., JAY GUO, Y. A wideband-to-narrowband tunable antenna using a reconfigurable filter. *IEEE Transactions on Antennas and Propagation*, 2015, vol. 63, no. 5, p. 2282–2285. DOI: 10.1109/TAP.2015.2402295

[12] SHARMA, S., TRIPATHI, C. C. Wideband to concurrent tri-band frequency reconfigurable microstrip patch antenna for wireless communication. *International Journal of Microwave and Wireless Technologies*, 2016, vol. 9, no. 4, p. 915–922. DOI: 10.1017/S1759078716000763

[13] SHARMA, S., TRIPATHI, C. C. A wide spectrum sensing and frequency reconfigurable antenna for cognitive radio. *Progress in Electromagnetics Research C*, 2016, vol. 67, p. 11–20. DOI: 10.2528/PIERC16070803

[14] SHARMA, S., TRIPATHI, C. C. A versatile reconfigurable antenna for cognitive radio. In *Proceedings of the Asia Pacific Microwave Conference (APMC 2016)*. New Delhi (India), 2016, 4 p. DOI: 10.1109/APMC.2016.7931320

[15] SHARMA, S., TRIPATHI, C. C., A novel reconfigurable antenna with spectrum sensing mechanism for CR system. *Progress in Electromagnetics Research C*, 2017, vol. 72, p. 187–196. DOI: 10.2528/PIERC17010901

About the Authors …

Sonia SHARMA received her M.Sc. degree in Electronics Science from Maharshi Dayanand University, Rohtak and M.Tech. in Electronics and Communication Engineering from UIET, Kurukshetra University, Kurukshetra. She is pursuing her Ph.D. in the area of reconfigurable antenna from UIET now.

Chandra Charu TRIPATHI received the B.Sc.(Honors-Physics) and M.Sc. (Solid State Electronics Devices) degrees from Banaras Hindu University, Varanasi, followed by Master in Engineering (Microelectronics) from BITS, Pilani, India. Presently, he is a Professor in the Department of Electronics and Communication Engineering at UIET, Kurukshetra University, Kurukshetra. He has more than 50 papers in refereed journals and 40 in national/ international conferences to his credit.